Bayesian Learning-Based Multi-Objective Distribution Power Network Reconfiguration

Tianwei Zhong, Hai-Tao Zhang, *Senior Member, IEEE*, Yuanzheng Li, *Member, IEEE*, Lan Liu, and Renzhi Lu, *Member, IEEE*

***Abstract*—This article proposes a scheme aiming at solving the reconfiguration problem of distribution power network (DPN) with high wind power penetrations. The virtue of the presented scheme lies in balancing the voltage stability and the absorption rate of wind energy. First, the DPN reconfiguration is formulated as a multi-objective optimization problem, where a curtailment strategy is introduced with the assistance of the secure operations of DPN. Thereby, the absorption rate of the generated wind power is maximized and voltage stability level is improved as well. Meanwhile, a modified multi-objective Bayesian learning-based evolutionary algorithm is applied to yield a Pareto front, which is a tradeoff between absorption rate and voltage stability. Afterwards, A technique for order preference by similarity to an ideal solution (TOPSIS) is adopted to determine the dispatching solution by similarity to an ideal solution. Finally, numerical case studies are conducted on a modified IEEE-33 bus system to verify the effectiveness of the proposed scheme.**

***Index Terms*—Wind power, distribution power network reconfiguration, multi-objective optimization, Bayesian learning.**

NOMENCLATURE

Abbreviations

DPN	Distribution power network
DPNR	Distribution power network reconfiguration
HV	Hyper-volume index
MD	Mean distance to reference point index
MMOBOA	Modified multi-objective Bayesian optimization algorithm
MOBOA	Multi-objective Bayesian optimization algorithm
MOP	Multi-objective optimization problem
SP	Spacing index
TOPSIS	Technique for order preference by similarity to an ideal solution

MMOBOA Parameters

$\mathcal{A}$	Additional archive
$\mathcal{G}(V, E)$	Bayesian network, a directed acyclic graph. V and E are vertices and edges in $\mathcal{G}$
$\mathcal{N}$	Non-dominated archive
M	Maximum iteration limit
$M_{\mathcal{A}}$	Capacity of $\mathcal{A}$
N	Number of particles in population
$n(*)$	The number of corresponding samples
$N_{\mathcal{A}}$	Number of solutions in $\mathcal{A}$
n_{v_i}, c_{π_i}	Number of possible values for v_i and π_i, $i = 1, 2, \ldots, n$
v_i, π_i	Vertex i and parent vertices of vertex i for the Bayesian network, $i = 1, 2, \ldots, n$

Power System Constants

$\boldsymbol{r_0}$	The reference point for MD and HV index
ε_{pf}	Tolerance of Newton-Raphson algorithm
K	Number of samples generated by scenario reduction
n	Number of tie switches
N_{B}, N_{E}	Number of buses and branches of DPN

Power System Variables

$\mathcal{S}$	Samples generated by scenario reduction
$\boldsymbol{A}$	Node-branch incidence matrix of DPNs
$\boldsymbol{x}$, $\boldsymbol{u}$	States and control signal of DPNR
ξ_r, ρ_r	Scenario r and corresponding possibility in $\mathcal{S}$, $r = 1, 2, \ldots, K$
C, V	Objectives of DPNR: curtailment of wind power and voltage deviation
G_{ij}, B_{ij}	Conductance and Susceptance between buses i and j, $i, j = 1, 2, \ldots, N_B$
H_i	The neighbors of bus i, $i = 1, 2, \ldots, N_B$
I_k	Current through branch k, $k = 1, 2, \ldots, N_E$
$I_k^{\max}$	Upper limit of I_k, $k = 1, 2, \ldots, N_E$
P_{ξ_r}, Q_{ξ_r}	Wind active and reactive output in ξ_r, $r = 1, 2, \ldots, K$
P_i, Q_i	Injected active and reactive at bus i, $i = 1, 2, \ldots, N_B$
P_{Li}, Q_{Li}	Active and reactive demand at bus i, $i = 1, 2, \ldots, N_B$

Manuscript received January 28, 2020; revised May 30, 2020 and August 23, 2020; accepted September 23, 2020. Date of publication September 29, 2020; date of current version February 26, 2021. This work was supported in part by the National Natural Science Foundation of China under Grant U1713203, Grant 51729501, Grant 62073148, and Grant 51721092; in part by the Guangdong Innovative and Entrepreneurial Research Team Program under Grant 2014ZT05G304; and in part by the Program for Core Technology Tackling Key Problems of Dongguan City under Grant 2019622101007. Paper no. TSG-00098-2020. *(Corresponding author: Hai-Tao Zhang.)*

Tianwei Zhong, Hai-Tao Zhang, Yuanzheng Li, and Renzhi Lu are with the School of Artificial Intelligence and Automation, Key Laboratory of Image Processing and Intelligent Control, and the State Key Laboratory of Digital Manufacturing Equipment and Technology, Huazhong University of Science and Technology, Wuhan 430074, China (e-mail: zht@mail.hust.edu.cn).

Lan Liu is with the National Engineering Laboratory for Educational Big Data, Central China Normal University, Wuhan 430079, China.

Color versions of one or more of the figures in this article are available online at https://ieeexplore.ieee.org.

Digital Object Identifier 10.1109/TSG.2020.3027290

V_i, θ_i Voltage amplitude and angle at bus i, $i = 1, 2, \ldots, N_B$

$V_i^{\min}$, $V_i^{\max}$ Lower and upper limit of V_i, $i = 1, 2, \ldots, N_B$

I. Introduction

DISTRIBUTION power network reconfiguration (DPNR) plays an essential role in distribution power networks (DPNs). The optimization of the inter-bus connections is beneficial to reduce power loss, and to enhance efficiency as well [1]–[3]. In recent decades, distributed generations (DGs) such as wind turbines and solar panels are widely deployed in DPNs, which contributes to both resource conservation and environmental protection. According to World Wind Energy Association (WWEA) [4], the capacity of wind power has reached 539291MW in 2018. In some western countries, e.g., Denmark, wind power takes an extremely high proportion, i.e., more than 40%. Thanks to the advanced grid connection techniques, a growing number of DGs have been embedded to DPNs [5] to improve the operational efficiency, and thereby to substantially reduce the operational cost of power grids.

Unfortunately, uncertainties of renewable energy have brought new challenges to the operation of DPNs [6]. To apply DPNR with integrated DGs, it is necessary to take these uncertainties into account [7], [8].

For instance, in [9], the power output of wind turbines is divided into several states, where each has its corresponding probability and hence could be used to calculate the objectives for DPNR process. As a milestone, [10] builds up a stochastic power output model of DGs. Therein, wind speed could be regarded as a probabilistic variable, and by this means, power loss has been considered in the objective function as well where Monte Carlo method could be adopted to maximize wind power absorption. Analogously, [11] establishes a scenario-based model, by which the mixed integer linear programming is utilized to minimize the reconfiguration costs. In this way, both power loss and voltage stability are improved. Along this research line, [12] uses a scenario reduction technique to deal with the stochastic issues in the scenario-based model, which effectively reduces the computation cost.

The above mentioned efforts have been devoted to deal with uncertainties generated by renewable energy, which show promising potential to reduce the adverse influences of the uncertainties in power grids. Along this research line, there are some works on the stochastic DPNR model [2], [13]–[15]. Specifically, [2] applies DPNR for congestion management with high penetration of distributed energy resources. Meanwhile, [2] contributes to both line loss reduction and voltage amplitude restraint which lead to low congestion management costs. Analogously, [13] considers wind power generators and thereby proposes a DPNR model to optimize energy loss, generation cost, emission and voltage deviation. Then, the four objectives are converted into a single one by an interactive fuzzy method. In this way, adaptive particle swarm optimization (APSO) is adopted, which show effectiveness of solving the single optimization problem. However, the quantitative relationship among these objectives has not been considered in APSO. Along this research line, [14] takes switching cost into consideration to prevent too many reconfigurations. However, too much curtailment still might be encountered in such schemes.

All of the above works consider the stochastic characteristic in the DPNR model. However, high renewable energy penetration may lead to intensified voltage instability [15], [16], which might cause a great damage to normal operations of DPNs. Therefore, it is necessary to guarantee voltage stability when higher wind power is introduced as well. These years have witnessed some efforts devoted to pursuing both voltage stability and high wind power penetrations. For instance, [17] claims that high wind power penetrations leads to overvoltage. As a remedy, curtailment is applied to assure voltage stability. In this way, [18] establishes a stochastic DPNR model and reconfigures the voltage stability as an optimization problem. Meanwhile, a modified particle swarm optimization (PSO) algorithm is adopted to optimize the network topology, which substantially improves the voltage stability.

Evidently, renewable energy is expected to be absorbed as much as possible [19] in current smart grids. Some research works have investigated high absorption rate-guaranteeing methodologies. For instance, [20] has enhanced the hosting capacity of DPNs so as to increase the absorption rate of renewable energy by DPNR. However, a large absorption rate of renewable energy would inevitably lead to poor voltage stability [15], [16]. A question is thus naturally inspired: what is the quantitative relationship between absorption rate and voltage stability? Till date, such dilemma has not been thoroughly studied, and thus has been left a challenging mission for renewable energy.

To this end, this article aims at establishing a multi-objective stochastic DPNR model, which balances the high absorption rate and voltage stability. Therein, we manifest the uncertainty of wind power by various samples via a scenario reduction method [12], [21], [22]. Then, we develop a modified multi-objective Bayesian optimization algorithm (MMOBOA) to address this problem. Accordingly, a Pareto front is achieved, which concretely quantifies the relationship between wind power absorption and voltage stability.

In summary, the contribution of this article is three-fold.

1) Propose a gradual curtailment strategy to estimate the absorption rate of DPNs.
2) Establish a multi-objective stochastic DPNR model to enhance the absorption rate of the high-renewable penetrated DPNs whereas maintaining the voltage stability.
3) Develop an MMOBOA to solve the stochastic DPNR problem, which achieves a high convergence rate using small population, compared with some existing mainstream evolutionary algorithms together with mixed integer programming.

The remainder of this article is organized as follows. Section II gives preliminaries and introduces the main problem. The multi-objective stochastic DPNR model is built up as well. Afterwards, MMOBOA is proposed in Section III with technical analysis. In Section IV, numerical simulations are conducted on benchmark systems to verify the

effectiveness of the proposed scheme. Finally, conclusion is drawn in Section V.

II. Problem Formulations

A. DPNR Model

First, the constrained optimization problem of DPNR is formulated as,

$$\min_{\boldsymbol{u}} \boldsymbol{F}(\boldsymbol{x}, \boldsymbol{u}, \mathcal{S}) \tag{1a}$$

$$\text{s.t.} \quad \det(\boldsymbol{A}) = \pm 1, \tag{1b}$$

$$V_i^{\min} \le V_i \le V_i^{\max}, \tag{1c}$$

$$|I_k| \le I_k^{\max}, \tag{1d}$$

$$P_i = V_i \Sigma_{j \in H_i} V_j (G_{ij} \cos(\theta_i - \theta_j) + B_{ij} \sin(\theta_i - \theta_j)), \tag{1e}$$

$$Q_i = V_i \Sigma_{j \in H_i} V_j (G_{ij} \sin(\theta_i - \theta_j) - B_{ij} \cos(\theta_i - \theta_j)), \tag{1f}$$

$$P_i = P_{\xi_r} - P_{Li}, \tag{1g}$$

$$Q_i = Q_{\xi_r} - Q_{Li}, \tag{1h}$$

where $\boldsymbol{F}$ is the objective function considering both wind power absorption and voltage deviation, $\boldsymbol{x} = [V_1, \ldots, V_{N_\mathrm{B}}, \theta_1, \ldots, \theta_{N_\mathrm{B}}]^\mathsf{T}$ denotes the system state, N_B is the number of buses, V_i and θ_i represent the magnitude and the angle of the voltage at bus i, respectively. $\boldsymbol{u} = [u_1, u_2, \ldots, u_n]^\mathsf{T}$ is the control variable, i.e., the set of tie switches for DPNR [23]–[25], and $\boldsymbol{S}$ is the set of wind power samples obtained by a scenario reduction method [21], [22] elaborated in Appendix A. Here, Eq. (1b) is the topology constraint. Eqs. (1c) and (1d) are the security constraints, whereas Eqs. (1e) and (1f) the power flow equations. Essentially, constraint (1b) implies that all the buses are connected with the root bus and no loops are allowable in the topology. Since wind generators are adopted here with a constant power factor, a group of DGs can be regarded as a PQ bus. Thus, the relationship between the injected power and the demand power are represented by Eqs. (1g) and (1h). Challengingly, the optimization problem (1) is non-convex [26], [27].

The curtailment of wind power could enhance the voltage stability of DNPs [17]. Nevertheless, an excess of curtailment leads to waste of energy resource. Therefore, in order to enhance the absorption rate of wind energy, [28] introduces a method to estimate the limit of curtailment. However, this limit varies with different scales of wind power, which is thus still arduous to be suitably picked. To solve this dilemma, we propose a gradual curtailment strategy with the assistance of secure operations of DPNs.

More precisely, the gradual curtailment procedure happens once some of the constraints (1b)-(1f) are activated. To better understand the gradual curtailment procedure, we exhibit the evolution of absorption γ along increasing scale α of maximum wind power absorption in Fig. 1. Initially, γ ascends linearly with increasing α, implying that no wind power is curtailed. Upon surpassing a threshold of 1.02, some constraint(s) in (1b)-(1f) are violated, which activates the curtailment. Hence, the gradual curtailment procedure is applied here. Taking $P_{\xi_i} = \gamma_0$ as an example, system states could be obtained via Eqs. (1e)–(1h). However, it is found that γ_0 is no longer feasible upon the violation of the constraints.

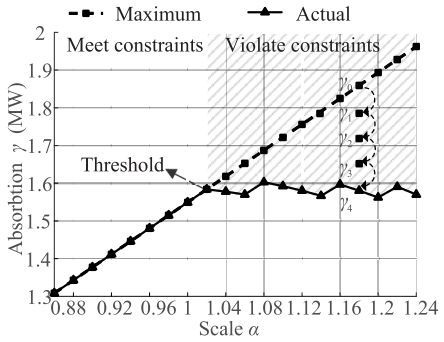

Fig. 1. The evolution of the absorption rate γ with increasing scale α of the wind power penetrates. Here, $\alpha = 1$ corresponds to 30% load demand. Unshaded and shaded regions denote inactivated and activated constraints, respectively.

Consequently, γ_0 is curtailed to γ_1 and hence some violation of constraints will be alleviated. In this way, γ_1 will iteratively decrease to γ_2, and then to γ_3, $\cdots$, and finally to γ_n until all the constraints in (1b)-(1f) are fulfilled. For instance, it is observed that $n = 4$ in Fig. 1. Once the gradual curtailment procedure terminates, the DPN is under the state of minimum curtailment and the objectives could be calculated as follows.

B. Objective Functions

Firstly, to enhance the absorption rate, it is essential to search for topologies with smaller curtailment. Taking the uncertainty of wind power into account, the network topology optimization problem could be formulated as

$$\min_{\boldsymbol{u}} C(\boldsymbol{x}, \boldsymbol{u}, \boldsymbol{S}) = \sum_{i=1}^{K} \rho_i C_i, \tag{2}$$

where ρ_i, C_i, K denote probability of scenario i, curtailment of wind power in scenario i and the number of remained scenarios, respectively.

Then, proper bus voltage is indispensable for secure operations in DPNs. Overvoltage and undervoltage are both harmful for the voltage stability, which necessitates the constraints on the voltage amplitudes. With the assistance of the voltage deviation estimation scheme [18], [29], we use a voltage observer formulated in (3) via the voltage derivation expectation of the DPNs. Therein, the uncertainties of wind power are addressed as below,

$$\min_{\boldsymbol{u}} V(\boldsymbol{x}, \boldsymbol{u}, \boldsymbol{S}) = \sum_{i=1}^{K} \rho_i \frac{1}{N_\mathrm{B}} \sum_{j=1}^{N_\mathrm{B}} |V_j - V_\mathrm{ref}|, \tag{3}$$

where V_ref denotes the reference value.

In addition, frequent switching is adverse to the tie switches, and total switching times is thus applied to estimate the operational cost [24] formulated as

$$\min_{\boldsymbol{u}} L(\boldsymbol{x}, \boldsymbol{u}, \boldsymbol{S}) = n(\boldsymbol{u} \cup \boldsymbol{u_0}) - n(\boldsymbol{u_0}), \tag{4}$$

where $n(\cdot)$ denotes the elements number of the set, and $\boldsymbol{u_0}$ the initial tie switches set. Thus, a stochastic multi-objective

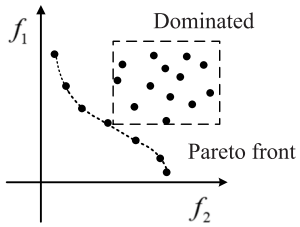

Fig. 2. Pareto solutions.

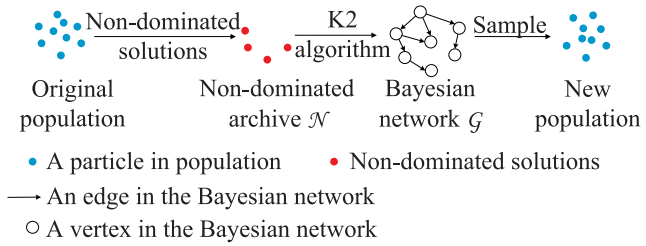

Fig. 3. Process of MOBOA.

optimization (MOP) problem is formulated as below

$$\begin{aligned} \min_{\boldsymbol{u}} \quad & [C(\boldsymbol{x},\boldsymbol{u},\boldsymbol{S}); V(\boldsymbol{x},\boldsymbol{u},\boldsymbol{S}); L(\boldsymbol{x},\boldsymbol{u},\boldsymbol{S})] \\ \text{s.t.} \quad & \text{(1b)–(1h)}, \end{aligned} \tag{5}$$

which synthetically considers wind power absorption rate, voltage stability and operational cost, and thus becomes the main objective pursued by the present study.

III. The Optimization Algorithm for DPNR

A. Pareto Solutions for an MOP

As introduced in [30], an MOP as formulation (5) could be generally formulated as

$$\begin{aligned} \min_{\boldsymbol{u}} \ & \boldsymbol{F}(\boldsymbol{u}), \\ \text{s.t.} \ & \boldsymbol{h}(\boldsymbol{u}) \le 0, \\ & \boldsymbol{g}(\boldsymbol{u}) = 0, \end{aligned} \tag{6}$$

where $\boldsymbol{F^i} = [F_1^i, F_2^i, \ldots, F_n^i]^\mathsf{T}$, $\boldsymbol{F^j} = [F_1^j, F_2^j, \ldots, F_n^j]^\mathsf{T}$ denote objectives of feasible solutions $\boldsymbol{u^i} = [u_1^i, u_2^i, \ldots, u_m^i]^\mathsf{T}$ and $\boldsymbol{u^j} = [u_1^j, u_2^j, \ldots, u_m^j]^\mathsf{T}$, respectively. To solve such a problem, multi-objective evolutionary computation algorithms are generally used. Conventionally, it could be converted into a single-objective optimization problem via some weighted sum method [31]. However, those methods do not work for the proposed DPNR model (1a)–(1h). On one hand, the weights selection are case by case, which are not easy to obtain. On the other hand, (5) is non-convex, which is arduous to find an analytic solution.

As a remedy, the method of non-dominated solutions and Pareto set have been introduced into the evolutionary algorithms, which is listed as follows.

- *Domination*: If $\forall k$, $F_k^i \le F_k^j$ and $\exists l$, $F_l^i < F_l^j$, $\boldsymbol{u^j}$ is said to be dominated by $\boldsymbol{u^i}$, i.e., $\boldsymbol{u^i} \preceq \boldsymbol{u^j}$. Moreover, $\boldsymbol{u^i}$ is a non-dominated solution if it is not be dominated by others. For instance, in Fig. 2, solutions inside the dashed box are dominated while the ones outside non-dominated;
- *Pareto set*: The Pareto set is composed of non-dominated solutions as $\mathcal{U} = \{\boldsymbol{u^1}, \boldsymbol{u^2}, \ldots, \boldsymbol{u^N}\}$;
- *Pareto front*: The multiple objectives of the Pareto set consist of the Pareto front as $\mathcal{P} = \{\boldsymbol{F^1}, \boldsymbol{F^2}, \ldots, \boldsymbol{F^N}\}$.

B. Multi-Objective Bayesian Optimization Algorithm

Meanwhile, multi-objective Bayesian optimization algorithm (MOBOA), a new multi-objective evolutionary computation algorithm, has also adopted non-dominated solutions to solve the MOP [32].

The iteration procedure of MOBOA is illustrated in Fig. 3, where MOBOA uses a population $\mathcal{U} = \{\boldsymbol{u_1}, \boldsymbol{u_2}, \ldots, \boldsymbol{u_{N_0}}\}$, i.e., N_0 candidate solutions to iteratively search for non-dominated solutions. Afterwards, all the non-dominated solutions are preserved in a non-dominated archive, denoted by $\mathcal{N}$. Then, MOBOA applies a Bayesian network $\mathcal{G} = \{V, E\}$ to estimate the joint probabilistic distribution of these non-dominated solutions [33]. Note that a vertex in V represents one dimension of $\boldsymbol{u}$ and an edge in E denotes the dependent two dimensions. Therein, K2 Algorithm [34] is used here to determine whether there is an edge between two vertices, which use the metric formulated as follows,

$$\text{Gain}(v_i, \pi_i) = \prod_{j=1}^{c_{\pi_i}} \frac{\Gamma(n_{v_i})}{\Gamma(n_{v_i} + n(\pi_i^j))} \prod_{k=1}^{n_{v_i}} \Gamma(1 + n(v_i^k, \pi_i^j)), \tag{7}$$

where v_i and π_i denote vertex i in V and the parent vertices of v_i, respectively; n_{v_i} is the number of possible values for v_i, and c_{π_i} represents that π_i has c_{π_i} possible values. In addition, $n(\cdot)$ stands for the number of corresponding samples in $\mathcal{N}$. If the existence of an edge leads to a larger gain, it is kept; otherwise, it will be removed from E. More specific information about K2 Algorithm could be referred to Appendix B. In this way, a Bayesian network encodes a joint probability distribution as below.

$$p(\boldsymbol{u}) \approx p(\mathcal{N}, \mathcal{G}) = \prod_{i=1}^{n} p(v_i | \pi_i), \tag{8}$$

where p is probability of vertex v_i with parent vertex π_i. Thereby, a new population is generated by hierarchically sampling the obtained Bayesian network. Specifically, the parent-free vertices are firstly handled, whose values are randomly generated. Afterwards, their child vertices could get the values according to the conditional probabilities. Once all the vertices are visited, a new sample is obtained.

C. Modified Multi-Objective Bayesian Optimization Algorithm

To better approximates the real distribution, $\mathcal{N}$ is required to capture adequate samples. To this end, MOBOA use a population with large N_0. For instance, [32] uses a population with hundreds particles, which however takes huge computation cost. The key challenge thus becomes obtaining sufficient samples just upon small population.

Traditionally, MOBOA obtains the Bayesian networks fitting non-dominated archive $\mathcal{N}$ as Eq. 8. However, $\mathcal{N}$ is updated with iterations, where repeated solutions and newly

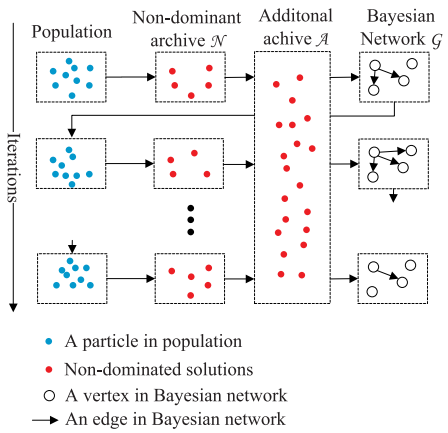

Fig. 4. The detailed procedure of MMOBOA.

dominated solutions would be removed from $\mathcal{N}$. Note that, these solutions however contribute little to establish the Bayesian network. Therefore, it is necessary to make full use of the information in these solutions to generated sufficient samples.

To fully utilize the information in these solutions of the original MOBOA, we design an additional archive $\mathcal{A}$ to preserve such solutions, namely, MMOBOA. Naturally, $\mathcal{A}$ has a limited capacity, denoted by $M_{\mathcal{A}}$. When $\mathcal{N}$ is obtained in each iteration, the number of non-dominated solutions in $\mathcal{A}$, denoted as $N_{\mathcal{A}}$, is assessed and $\mathcal{A}$ is updated according to the following rules,

- $N_{\mathcal{A}}$ is less than $M_{\mathcal{A}}$, then $\mathcal{A} \leftarrow \mathcal{A} \cup \mathcal{N}$;
- Otherwise, $N_{\mathcal{A}} - M_{\mathcal{A}}$ dominated solutions are removed from $\mathcal{A}$. Then, $\mathcal{A} \leftarrow \mathcal{A} \cup \mathcal{N}$.

Thereafter, MMOBOA applies a Bayesian network to estimate the joint probabilistic distribution of solutions in $\mathcal{A}$ formulated as follows,

$$p(\boldsymbol{u}) \approx p(\mathcal{A}, \mathcal{G}) = \prod_{i=1}^{n} p(v_i|\pi_i). \tag{9}$$

The process of MMOBOA is illustrated in Fig. 4. Analogously, MMOBOA uses a population $\mathcal{U} = \{\boldsymbol{u_1}, \boldsymbol{u_2}, \ldots, \boldsymbol{u_N}\}$ to search for non-dominated solutions, in which $N \ll N_0$. Non-dominated solutions selected from the population are preserved in non-dominated archive $\mathcal{N}$. Then, the additional archive $\mathcal{A}$ keeps a copy of $\mathcal{N}$. Meanwhile, the number of solutions in $\mathcal{A}$ is checked via above two rules. Afterwards, a Bayesian network encodes the joint probability distribution of $\mathcal{A}$ and the new population is also sampled from obtained Bayesian network. Repeat the above process until the maximum iteration is reached. Finally, the non-dominate solutions in $\mathcal{N}$ make up the approximate Pareto set. It is observed from Fig. 4 that solutions are only removed from $\mathcal{A}$ when the maximum capacity is reached. Thus, some feasible solutions might have multiple copies in $\mathcal{A}$. In this way, one could get adequate samples to establish Bayesian networks upon acceptable computation.

To apply MMOBOA to the DPNR model (1a)–(1h), the calculation of objectives is necessary. Note that all the objectives are computed under the state of minimum curtailment detailed in Algorithm 1. After terminates at the minimum curtailment, the objectives could be accordingly calculated as (2) (3) and (4), respectively.

Algorithm 1 Gradual Curtailment

- Initialize curtailment $C_i = 0$;
- **Step 1**: If $P_{\xi_i} > 0$, go to step 2. Otherwise, go to step 7;
- **Step 2**: Substitute P_{ξ_i} and Q_{ξ_i} into Eqs. (1g) and (1h), respectively. Calculate actual injected active power P_i^* and reactive power Q_i^*;
- **Step 3**: Replace P_i and Q_i with P_i^* and Q_i^* in Eqs. (1e)-(1f), respectively. Solve the power flow equations via Newton-Raphson algorithm and obtain the values of system states $\boldsymbol{x}$;
- **Step 4**: Substitute $\boldsymbol{x}$ into Eqs. (1e)-(1f) and obtain calculated injected power P_i^s and Q_i^s, respectively;
- **Step 5**: If the values of $|P_i^s - P_i^*|$ and $|Q_i^s - Q_i^*|$ are both smaller than given tolerance ε_{pf} and $\boldsymbol{x}$ fulfills constraints (1c)-(1d), go to step 7. Otherwise, curtail active wind power and a new integrated power output P'_{ξ_i} is yielded;
- **Step 6**: Update $C_i = C_i + (P_{\xi_r} - P'_{\xi_r})$, $P_{\xi_r} = P'_{\xi_r}$ and return to step 1;
- **Step 7**: If the values of $|P_i^s - P_i^*|$ and $|Q_i^s - Q_i^*|$ are both smaller than given tolerance ε_{pf} and solution $\boldsymbol{x}$ meet constraints (1c)-(1d), $C_i = \inf$. Otherwise, keep C_i.

Algorithm 2 Solve Proposed DPNR Model With MMOBOA

- **Step 1**: Load buses and branches data of the DPN. Set the tolerance of Newton-Raphson algorithm ε_{pf} and maximum iteration times is M;
- **Step 2**: Generate K wind power samples $\mathcal{S}$ via scenario reduction elaborated in Appendix A;
- **Step 3**: Randomly initialize $\mathcal{U} = \{\boldsymbol{u_1}, \boldsymbol{u_2}, \cdots, \boldsymbol{u_N}\}$. Set $\mathcal{N} = NULL$, $\mathcal{A} = NULL$ and $m = 1$;
- **Step 4**: Set $j = 1$;
- **Step 5**: Change the topology of DPN by open the tie switches in $\boldsymbol{u_j}$;
- **Step 6**: For each sample in $\mathcal{S}$, apply gradual curtailment via Algorithm 1. Calculate expectations of curtailment of wind power and voltage deviation via Eqs. (2) and (3), respectively;
- **Step 7**: Set $j = j + 1$. If $j = N$, go to step 8. Otherwise, go to step 5;
- **Step 8**: Selected Pareto solutions as Appendix B and update $\mathcal{N}$. Update $\mathcal{A} = \mathcal{A} \cup \mathcal{N}$ and check the number of solutions in $\mathcal{A}$ via the above two rules;
- **Step 9**: Establish $\mathcal{G}$ fitting $\mathcal{A}$ via K2 Algorithm [34]. Sample N new solutions $\{\boldsymbol{u_1}, \boldsymbol{u_2}, \cdots, \boldsymbol{u_N}\}$ from obtained $\mathcal{G}$ and replace $\mathcal{U}$ with them;
- **Step 10**: Set $m = m + 1$. If m reaches M,go to step 11 Otherwise, go to step 4;
- **Step 11**: Apply the technique for order preference by similarity to an ideal solution (TOPSIS) [35] to choose solution from $\mathcal{N}$. The selected one is the final dispatching solution.

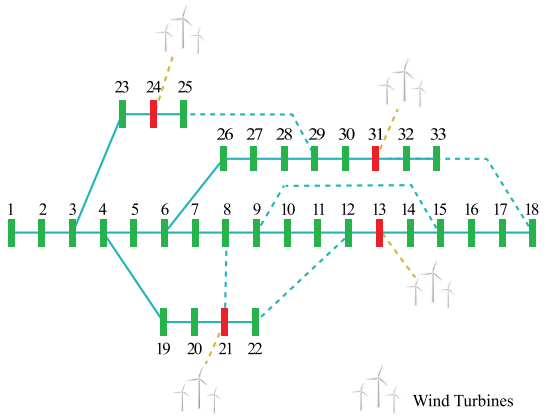

Fig. 5. Modified IEEE-33 system.

The procedure of DPNR is detailed as Algorithm 2. Initially, it can be observed that a scenario-reduction method is used to generate various wind power samples. Then, we adopt the method proposed in [24] to randomly initialize the population, where each particle represents a candidate solution. Specifically, for each fundamental loop of DPNs, the tie switch is randomly picked, whose corresponding branch is thus disconnected. Meanwhile, the non-dominated archive $\mathcal{N}$ and the additional archive $\mathcal{A}$ are initialized. In each iteration, each particle is used to calculate curtailment of wind power and voltage deviation. Afterwards, $\mathcal{N}$ and $\mathcal{A}$ are updated. Then, a Bayesian network $\mathcal{G}$ is used to estimate the joint probabilistic distribution of $\mathcal{A}$ via K2 Algorithm. At the end of each iteration, a new population is sampled from $\mathcal{G}$. If iteration times reaches the threshold, the process of MMOBOA terminates and the Pareto set, i.e., $\mathcal{N}$ is obtained in the final iteration. It is noteworthy that we use technique for order preference by similarity to an ideal solution (TOPSIS) [35] to make the final decision, which is the dispatching solution of the proposed stochastic DPNR model.

IV. Case Studies

A. Simulation Settings

We conduct case studies on a modified IEEE-33 system [10] shown in Fig. 5, which consists of 33 buses and 37 branches. Therein, each wind turbine is assumed to have an identical dynamics, i.e., double-fed induction generator with a constant power factor. Specifically, its rated power is 17.5 KW, and the cut-in, rated, cut-out speeds are 4 m/s, 12.5 m/s and 20 m/s, respectively. The number of wind power samples after the scenario reduction is set as 30.

To demonstrate the merit of the proposed MMOBOA, we have applied four mainstream optimization algorithms summarized in [36] to the DPNR model as well for comparison. These closely-related algorithms include multi-objective particle swarm optimization (MOPSO), multi-objective evolutionary algorithm based on decomposition (MOEA/D), strength Pareto evolutionary algorithm II (SPEA-II) and non-dominated sorting genetic algorithm II (NSGA-II). Specifically, the performances of these five algorithms are compared in 30 independent runs. As for Newton-Raphson algorithm carried out by the software of MATPOWER [37], ε_{pf} is set as 10^{-6} (p.u.). In addition, we identically set the size of population N as 30 and the number of maximum iteration M as 300. Regarding MMOBOA, the capacity $M_{\mathcal{A}}$ of the additional archive $\mathcal{A}$ is 1000, so as to accommodate sufficient historical non-dominated solutions.

TABLE I
The Predicted Wind Speeds and Number of Wind Turbines at Each Bus

Bus No.	13	21	24	31
Wind speed (m/s)	7.6	9.3	8.7	15
Turbines number	30	30	30	30

As for the metric comparison of the these evolutionary algorithms, we use four indices, i.e., the hyper-volume (HV), the mean distance (MD), the spacing (SP) index and the scale of Pareto front [38], [39]. More precisely, HV is the volume covered by the non-dominated solutions when the reference point is given, which is an index to assess both the convergence and the diversity of obtained Pareto fronts. MD represents the mean Euclidian distance between Pareto front and the reference point, which represents the convergence of algorithms. SP is adopted to estimate diversity whereas searching efficiency index is quantified by the number of solutions with respect to Pareto set (NSPS). Moreover, HV, MD and SP indices are, respectively, calculated by Eqs. (10a)-(10c),

$$\mathrm{HV}(\mathcal{N}, \boldsymbol{r_0}) = \cup_{i=1}^{N_{\mathcal{N}}} \mathrm{Vol}(\boldsymbol{F}(\boldsymbol{u_i}), \boldsymbol{r_0}), \tag{10a}$$

$$\mathrm{MD}(\mathcal{N}, \boldsymbol{r_0}) = \frac{1}{N} \sum_{i=1}^{N} \|\boldsymbol{F}(\boldsymbol{u_i}) - \boldsymbol{r_0})\|_2, \tag{10b}$$

$$\mathrm{Spacing}(\mathcal{N}) = \frac{1}{N-1} \sum_{i=1}^{N-1} \|\boldsymbol{F}(\boldsymbol{u_i}) - \boldsymbol{F}(\boldsymbol{u_{i+1}})\|_2, \tag{10c}$$

where $\boldsymbol{r_0}$ is the reference point, $N_{\mathcal{N}}$ is the number of solutions in $\mathcal{N}$, and $\mathrm{Vol}(\cdot)$ is the volume between two points. Therefore, a greater NSPS value indicates superior searching ability of the algorithms, larger HV and MD values imply a better convergent Parent front, whereas a smaller SP value corresponds to a well-distributed Pareto front. Accordingly, a good solution selection is a compromise between a quick convergent rate and a nicely-distributed Pareto front.

In addition, mixed integer programming (MIP) is commonly used to handle with DPNR models. Especially, it has the merit that local optimal solution is guaranteed [40]. Therefore, MIP is also applied to proposed DPNR model. Therein, the weighted sum method is used to combine the objectives and the weights are all equal. Specifically, it is implemented in GAMS and the MINLP solver SBB is used to solve the model.

As shown as Fig. 5, the voltage amplitude $[V_i^{\min}, V_i^{\max}]$ defined in Eq. (1) is supposed to maintain within the scope of [0.9, 1.1]. In addition, wind turbines are supposed to install on the buses 13, 21, 24 and 31. The predicted wind speeds at each bus and corresponding number of wind turbines are listed in Tab I. Note that each bus is connected with 10 wind turbines.

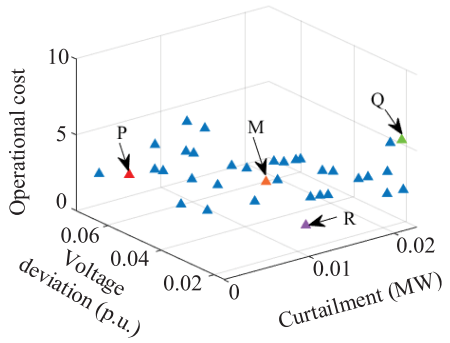

Fig. 6. The best Pareto fronts distribution obtained by MMOBOA.

TABLE II
THE OBJECTIVE FUNCTIONS OF INITIAL STATE AND DPNR

	Open switches	Curtailment (KW)	Voltage deviation (p.u.)
Initial values	8-21, 9-15, 12-22, 18-33, 25-29	14.7	0.0323
DPNR	8-21, 9-15, 11-12, 21-22, 23-24	9.1	0.0292

Moreover, the standard deviation of wind speed prediction error is set to 8% of corresponding forecasted speed.

B. Simulation Results and Analysis

The best Pareto fonts obtained by MMOBOA are shown Fig. 6. Upon obtaining sufficient solutions, TOPSIS is applied for decision making. As shown in Fig. 6, solution M with coordinate $(0.0091, 0.0292, 4)$ is selected. In order to verify the performance of solution M, we make comparison with the extreme cases, i.e., the solution P $(0, 0.0520, 4)$, Q $(0.0209, 0.0159, 6)$ and R $(0.0147, 0.0323, 0)$, respectively. Therein, the curtailment of solution P is 0, which maximizes the absorption rate of wind power. However, the large expectation of voltage deviation could lead to voltage instability. On the contrary, solution Q has the merit of minimizing the voltage deviation, which is however at the cost of a small share of wind power. Moreover, solution R minimizes the number of switching. Thereby, the topology of the DPN remains unchanged. As a remedy, solution M considers absorption rate, voltage stability and number of switching, which is a suitable tradeoff among these three objectives.

In order to investigate the performance of DPNR, Table II lists two objective functions of the initial states and DPNR. It is observed that the curtailment of wind power is 147kW under the initial state case, which is much larger than that of DPNR. Meanwhile, the voltage deviation has been decreased from 0.0323 to 0.0292. Therefore, DPNR increases the absorption rate of wind power whereas keeping the voltage stable, which is desirable in real applications.

Moreover, Fig. 7 shows the system states and corresponding variations. It is observed that no constraints (including the most important voltage security constraint) are violated, which verified the effectiveness of proposed stochastic DPNR model.

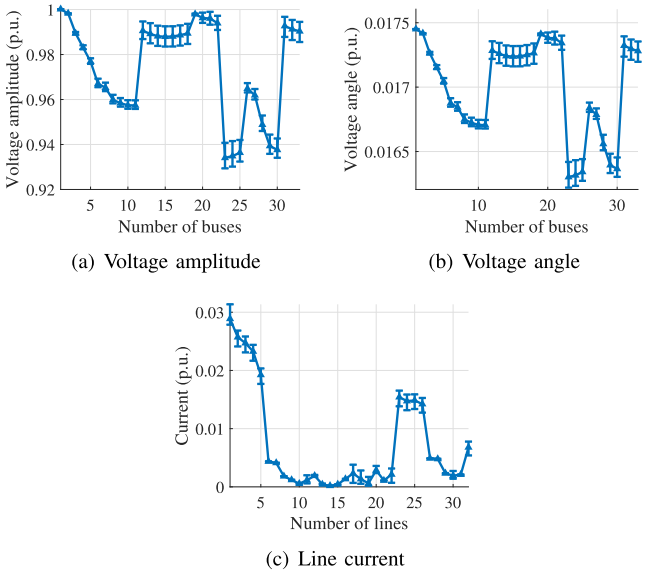

(a) Voltage amplitude (b) Voltage angle

(c) Line current

Fig. 7. The evolution of system states, i.e., Voltage amplitude, voltage angle and line current, along increasing number of buses.

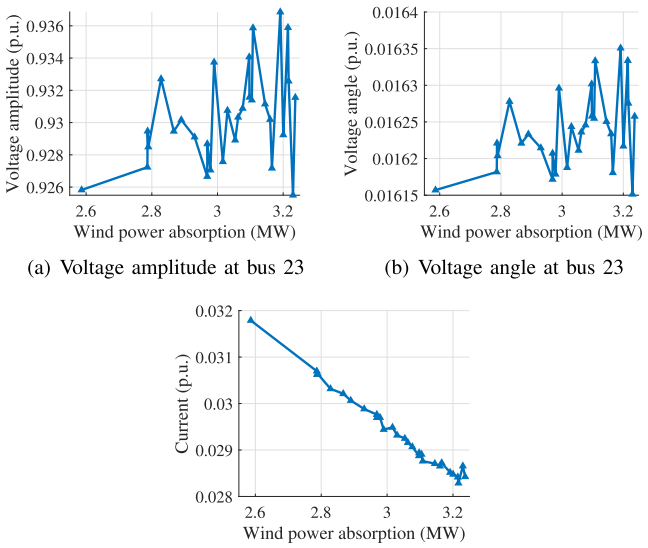

(a) Voltage amplitude at bus 23 (b) Voltage angle at bus 23

(c) Line current at line 1

Fig. 8. The variation of system states corresponding to wind power absorption.

To show the relationships among above system states and wind power curtailment, we choose the states with large variance, i.e., voltage amplitude of bus 23, voltage angle of bus 23 and line current at line 1. Fig. 8 demonstrates their variation as wind power absorption increases. It is observed that all of the selected states have nonlinear relationships with wind power absorption for the complexity of power flow equations.

To further verify the effectiveness of the stochastic DPNR model, we further conduct DPNR and MMOBOA with fixed forecasted wind speed. Fig. 9 shows the voltage deviation of 33 buses corresponding to 30 wind power samples. Recall that the voltage amplitude V_i should be keep in the scope of [0.9, 1.1]. If only considering forecasted wind speed, the voltage deviation will grow larger, which always leads to unstable

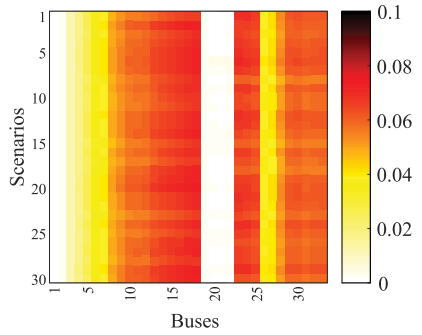

(a) DPNR with fixed forecasted wind speed

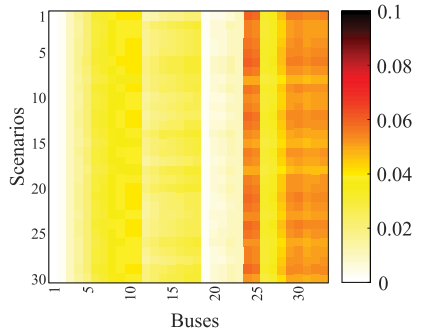

(b) Stochastic DPNR with prediction error

Fig. 9. Voltage deviation comparison between the routine DPNR and the present stochastic DPNR over dispatching solutions corresponding to 30 remained wind power samples. Smaller voltage deviation (lighter color) indicate superior voltage stability.

TABLE III
THREE PARETO FRONTS' DISTRIBUTION COMPARISON OF THE FIVE ALGORITHMS

	SP	$x-z$	$x-y$	$y-z$
MMOBOA	**2.2944**	**0.0318**	**4.2286**	0.0099
MOPSO	2.6672	0.0344	6.0500	0.0113
MOEA/D	3.0000	0.0415	5.3333	**0.0091**
SPEA-II	2.4667	0.0323	4.2581	0.0098
NSGA-II	3.0012	0.0358	5.8462	0.0115

voltages. Specifically, the voltage deviation of bus 30 is 0.1, which is about to violate the secure constraints. In comparison, by using the present stochastic DPNR, one obtains more stable voltage, whose amplitudes keep larger than 0.92. Therefore, the uncertainties of wind speed should be taken into account when establishing DPNR.

C. Comparison With Other Evolutionary Algorithms

To compare MMOBOA with other four algorithms (i.e., MOPSO, MOEA/D, SPEA-II and NSGA-II), Table III lists the mean distances between Pareto set and panels as well as the SP index, where the minimal values are marked bold. Remarkably, MMOBOA almost keep the closest distances to all the $x-z$, $x-y$, $y-z$ planes (just a little bit higher than MOEA/D to $y-z$ plan), which indicates it has lower curtailment of wind power and lower voltage deviation. Meanwhile,

TABLE IV
HV, MD AND NSPS COMPARISON OF THE FIVE ALGORITHMS

	HV	MD	NSPS
MMOBOA	**1.6877**	**5.9109**	**35**
MOPSO	1.2370	4.2029	34
MOEA/D	0.2938	4.8647	3
SPEA-II	1.0305	5.8833	31
NSGA-II	0.5226	4.5587	13

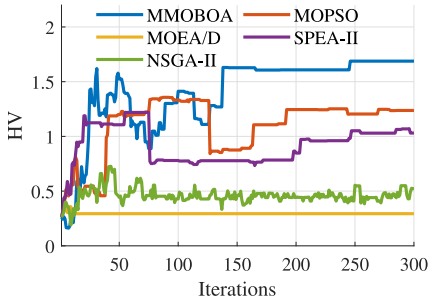

Fig. 10. HV evolution comparison of the five algorithms (i.e., MMOBOA, MOPSO, MOEA/D, SPEA-II and NSGA-II) along increasing iterations.

lower SP indicates these solutions are more evenly distributed. Therefore, MMOBOA beats other algorithms in searching for evenly distributed solutions.

To quantify the Pareto fronts of the algorithms under investigation, the reference point $\boldsymbol{r_0}$ is set to $(1.2, 0.15, 10)$, which could also be replaced by other points. The comparison of three indicators is listed in Table IV. More precisely, regarding HV, MMOBOA has the largest value which indicates it converges to the Pareto front most quickly. Meanwhile, high MD of MMOBOA implies more convergent Pareto optimal solutions. MMOBOA obtains 35 solutions, which is close to MOPSO and is larger than that of other approaches. Thus, the searching superiority of MMOBOA is verified.

We compare the HV evolution of the five algorithms over 30 independent runs in Fig. 10. It is observed that MMOBOA obtain the best nondominated solution distribution as it finally gets the largest HV value. Moreover, MMOBOA obtains these solutions within 250 iterations whereas MOPSO within 270, MOEA/D within 10, SPEA-II within 290 and NSGA-II within 300, respectively. Although MOEA/D converges to the approximate Pareto front more quickly, the obtained solutions are unacceptable as they are much less convergent. Regarding the objective of achieving learning stability via small population size N scenarios, the merit of using additional archive in MMOBOA is thus verified.

To further show the virtue of the proposed MMOBOA, we compare its optimal solutions of three objectives with a mainstream algorithm MIP in Tab V. It is observed that MMOBOA outperforms MIP as the objectives of the former are closer to those of the latter under a same initial state. This implies that MIP is more likely to be trapped in local optima. Moreover, to obtain the Pareto front, MIP needs to handle various combinations of weights, which requires multiple runs. As

TABLE V
THE OBJECTIVE FUNCTIONS OF DISPATCH SOLUTIONS OBTAINED BY MMOBOA AND MIP

	Curtailment (KW)	Voltage deviation (p.u.)	Operation cost
Initial values	14.7	0.0323	/
MMOBOA	9.1	0.0292	6
MIP	14.7	0.0340	8

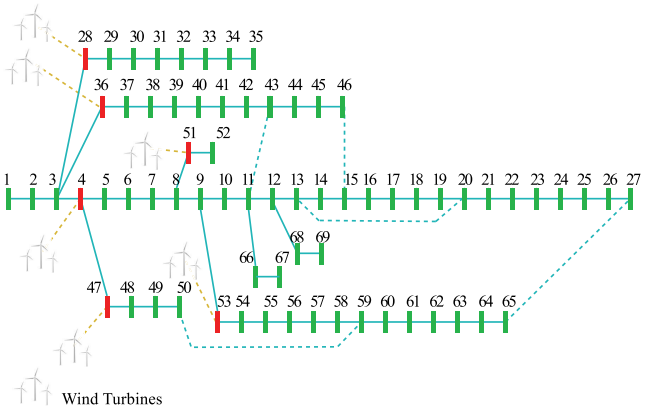

Fig. 11. Modified IEEE-69 system.

TABLE VI
THE OBJECTIVE FUNCTIONS OF INITIAL STATE AND DPNR FOR THE MODIFIED IEEE-69 SYSTEM

	Open switches	Curtailment (KW)	Voltage deviation (p.u.)
Initial values	11-43, 13-20, 15-46, 27-65, 50-59	109	0.0712
DPNR	4-5, 13-20, 15-46, 27-65, 50-59	71	0.0582

the dimension of objectives grows, the possible combinations increases exponentially. Thus, if high absorption rate is pursued as the present study, MMOBOA should be the better choice. However, if it suffices to get a feasible solution, MIP is more preferable, as it finds such a solution more quickly than MMOBOA (3s VS 65s).

D. Scaling Test: Simulations on a Large System

To show the generality of the present scheme, we conduct numerical simulations on a larger benchmark system, i.e., a modified IEEE-69 system consisting of 69 buses and 73 branches as shown in Fig. 11. The wind turbines are installed on the buses 4, 28, 36, 47, 51 and 53 with corresponding predicted wind speeds of 11.5 , 6.8, 7.1, 9.2, 8.3 and 9.5 m/s, respectively. Other parameters are set the same as those of IEEE-33 system.

The objectives under a prescribed initial state and DPNR are listed in Tab VI. It surfaces that both the absorption rate and voltage stability are enhanced via two switching operations. From the efficiency point of view, MMOBOA completes 300 iterations with 145 seconds. Compared to 65 seconds of IEEE-33 system with 33 buses and 37 branches, the calculation efficiency of MMOBOA keeps high as well. Thus, the generality of the proposed model is verified.

V. CONCLUSION

This article proposes a stochastic DPNR model which compromises absorption rate of wind power and voltage stability. Thereby, a Bayesian learning-based evolutionary algorithm, i.e., MMOBOA, is developed to search for the optimal Pareto fronts. Case studies conducted on modified IEEE-33 and IEEE-69 systems manifest that, the proposed scheme guarantees high penetration rate of wind power and maintains stable voltage. Moreover, the superiority of the present MMOBOA in terms of searching for Pareto set is intensified for smaller sized population.

APPENDIX A
SCENARIO REDUCTION FOR GENERATING WIND POWER SCENARIOS

Wind speed is calculated through forecasted speed and prediction error [41]. Prediction error is supposed to obey Gaussian distribution, which has expectation 0 and standard deviation σ. Wind speed can be formulated as follows.

$$v = v_{\text{ref}} + v_{\text{err}}, \quad v_{\text{err}} \sim N(0, \sigma^2), \tag{11}$$

where v_{ref} is the forecasted speed and v_{err} denotes the corresponding prediction error.

Once wind speed is obtained, the output of wind turbines can be calculated through the following equation [42].

$$P = \begin{cases} 0, & v < v_{\text{in}}, \\ (a + bv^3), & v_{\text{in}} \le v < v_{\text{ra}}, \\ P_{\text{ra}}, & v_{\text{ra}} \le v < v_{\text{out}}, \\ 0, & v \ge v_{\text{out}}, \end{cases} \tag{12}$$

where $a = \frac{P_{\text{ra}} v_{\text{in}}^3}{v_{\text{ra}}^3 - v_{\text{in}}^3}$, $b = \frac{P_{\text{ra}}}{v_{\text{ra}}^3 - v_{\text{in}}^3}$. v_{in}, v_{out}, v_{ra} are cut-in, cut-out and rated speeds, respectively, and P_{ra} is the rated active power output.

When wind turbines connect with DPNs, the influence of reactive output can not be ignored either. Here, we adopt wind turbines with constant power factor $\cos\varphi$. Thus, the corresponding reactive power could be evaluated as $Q = P\frac{\sqrt{1-\cos^2\varphi}}{\cos\varphi}$.

In [9]–[11], Monte Carlo methods are applied to generating wind power scenarios. Analogously, this article adopts Latin hypercube sampling with Cholesky decomposition (LHS-CD) [43]. More precisely, N initial scenarios $\mathcal{S}_0 = \{\xi_1, \xi_2, \ldots, \xi_N\}$ are generated according to the wind power model. For each scenario ξ_i, it is composed of the wind power output P_{ξ_i}, Q_{ξ_i} and their corresponding probability ρ_i. To avoid the heavy calculation burden on large initial scenarios number N, scenario reduction is used [21], [22]. We picks K representative scenarios $\mathcal{S} = \{\xi_1, \xi_2, \ldots, \xi_K\}$, in which $K \ll N$.

Algorithm 3 shows the procedure of K2 Algorithm, which is used to obtain the edges of a Bayesian network. Here, $\mathcal{A}$ denotes the database.

Algorithm 3 K2 Algorithm

- **Step 1**: Initialize the edge set $E = NULL$. Input database D, a set V with n vertices;
- **Step 2**: Set $i = 1$;
- **Step 3**: Initialize the parent set and the candidate parent set as $\pi_i = NULL$ and $z_i = V$, respectively;
- **Step 4**: Calculate Gain_{old};
- **Step 5**: Select the vertex v_j that maximizes $\text{Gain}(v_i, \pi_i \cup \{v_j\})$;
- **Step 6**: Calculate $\text{Gain}_{\text{new}}(v_i, \pi_i \cup \{v_j\})$;
- **Step 7**: If $\text{Gain}_{\text{new}} > \text{Gain}_{\text{old}}$, set $\text{Gain}_{\text{old}} = \text{Gain}_{\text{new}}$, $z_i = z_i - \{v_j\}$, $E = E \cup \{v_j \to v_i\}$ and $\pi_i = \pi_i \cup \{v_j\}$, and then go to step 8. Otherwise, go to step 9;
- **Step 8**: If $z_i = NULL$, go to step 8. Otherwise, go to step 5;
- **Step 9**: Set $i = i + 1$. If $i > n$, go to step 9. Otherwise, go to step 3;
- **Step 10**: Output the edge set E.

REFERENCES

[1] Y. Liu, J. Li, and L. Wu, "Coordinated optimal network reconfiguration and voltage regulator/der control for unbalanced distribution systems," *IEEE Trans. Smart Grid*, vol. 10, no. 3, pp. 2912–2922, Mar. 2018.

[2] F. Shen, S. Huang, Q. Wu, S. Repo, Y. Xu, and J. Ostergaard, "Comprehensive congestion management for distribution networks based on dynamic tariff, reconfiguration, and re-profiling product," *IEEE Trans. Smart Grid*, vol. 10, no. 5, pp. 4795–4805, Sep. 2019.

[3] Y. Wang, Z. Huang, M. Shahidehpour, L. L. Lai, Z. Wang, and Q. Zhu, "Reconfigurable distribution network for managing transactive energy in a multi-microgrid system," *IEEE Trans. Smart Grid*, vol. 11, no. 2, pp. 1286–1295, Mar. 2020.

[4] WWEA. (2018). *Wind Power Capacity Worldwide Reaches 600 GW, 53,9 GW Added in 2018*. [Online]. Available: https://wwindea.org/blog/2019/02/25/wind-power-capacity-worldwide-reaches-600-gw-539-gw-added-in-2018/

[5] WWEA. *Another Record Breaking Year for Renewable Energy: More Renewable Energy Capacity for Less Money*. [Online]. Available: https://wwindea.org/blog/2017/06/07/another-record-breaking-year-for-renewable-energy-more-renewable-energy-capacity-for-less-money/

[6] F. Blaabjerg and K. Ma, "Wind energy systems," *Proc. IEEE*, vol. 105, no. 11, pp. 2116–2131, Nov. 2017.

[7] W. Sun, M. Zamani, H.-T. Zhang, and Y. Li, "Probabilistic optimal power flow with correlated wind power uncertainty via Markov chain quasi-Monte-Carlo sampling," *IEEE Trans. Ind. Informat.*, vol. 15, no. 11, pp. 6058–6069, Jul. 2019.

[8] W. Sun, M. Zamani, M. R. Hesamzadeh, and H.-T. Zhang, "Data-driven probabilistic optimal power flow with nonparametric Bayesian modeling and inference," *IEEE Trans. Smart Grid*, vol. 11, no. 2, pp. 1077–1090, Mar. 2020.

[9] J. Shukla, B. Das, and V. Pant, "Stability constrained optimal distribution system reconfiguration considering uncertainties in correlated loads and distributed generations," *Int. J. Elect. Power Energy Syst.*, vol. 99, pp. 121–133, Jul. 2018.

[10] H. Wu and P. Dong, "PPSO method for distribution network reconfiguration considering the stochastic uncertainty of wind turbine, photovoltaic and load," *J. Eng.*, vol. 2017, no. 13, pp. 2032–2036, 2017.

[11] A. W. Bizuayehu, A. A. S. de la Nieta, J. Contreras, and J. P. Catalao, "Impacts of stochastic wind power and storage participation on economic dispatch in distribution systems," *IEEE Trans. Sustain. Energy*, vol. 7, no. 3, pp. 1336–1345, Jul. 2016.

[12] M. Nick, R. Cherkaoui, and M. Paolone, "Optimal planning of distributed energy storage systems in active distribution networks embedding grid reconfiguration," *IEEE Trans. Power Syst.*, vol. 33, no. 2, pp. 1577–1590, Aug. 2018.

[13] A. R. Malekpour, T. Niknam, A. Pahwa, and A. K. Fard, "Multi-objective stochastic distribution feeder reconfiguration in systems with wind power generators and fuel cells using the point estimate method," *IEEE Trans. Power Syst.*, vol. 28, no. 2, pp. 1483–1492, Oct. 2013.

[14] M. R. Dorostkarghamsari, M. Fotuhifiruzabad, M. Lehtonen, A. Safdarian, and A. S. Hoshyarzade, "Stochastic operation framework for distribution networks hosting high wind penetrations," *IEEE Trans. Sustain. Energy*, vol. 10, no. 1, pp. 344–354, Oct. 2019.

[15] M. Zeraati, M. E. H. Golshan, and J. M. Guerrero, "Distributed control of battery energy storage systems for voltage regulation in distribution networks with high PV penetration," *IEEE Trans. Smart Grid*, vol. 9, no. 4, pp. 3582–3593, Dec. 2018.

[16] Y. Li *et al.*, "Study on voltage control in distribution network with renewable energy integration," in *Proc. IEEE Conf. Energy Internet Energy Syst. Integr. (EI2)*, 2017, pp. 1–5.

[17] S. Chalise, H. R. Atia, B. Poudel, and R. Tonkoski, "Impact of active power curtailment of wind turbines connected to residential feeders for overvoltage prevention," *IEEE Trans. Sustain. Energy*, vol. 7, no. 2, pp. 471–479, Dec. 2016.

[18] H. Wu, P. Dong, and M. Liu, "Distribution network reconfiguration for loss reduction and voltage stability with random fuzzy uncertainties of renewable energy generation and load," *IEEE Trans. Ind. Informat.*, vol. 16, no. 9, pp. 5655–5666, Sep. 2020.

[19] M. O'Malley, "Grid integration [in my view]," *IEEE Power Energy Mag.*, vol. 9, no. 6, pp. 120–128, Oct. 2011.

[20] Y. Zheng, Z. Y. Dong, F. J. Luo, K. Meng, J. Qiu, and K. P. Wong, "Optimal allocation of energy storage system for risk mitigation of discos with high renewable penetrations," *IEEE Trans. Power Syst.*, vol. 29, no. 1, pp. 212–220, Sep. 2014.

[21] Y. Xu, Z. Y. Dong, R. Zhang, and D. J. Hill, "Multi-timescale coordinated voltage/var control of high renewable-penetrated distribution systems," *IEEE Trans. Power Syst.*, vol. 32, no. 6, pp. 4398–4408, Feb. 2017.

[22] H. Heitsch and W. Römisch, "Scenario reduction algorithms in stochastic programming," *Comput. Optim. Appl.*, vol. 24, nos. 2–3, pp. 187–206, 2003.

[23] A. M. Eldurssi and R. M. O'Connell, "A fast nondominated sorting guided genetic algorithm for multi-objective power distribution system reconfiguration problem," *IEEE Trans. Power Syst.*, vol. 30, no. 2, pp. 593–601, Jul. 2015.

[24] T. T. Nguyen, T. T. Nguyen, A. V. Truong, Q. T. Nguyen, and T. A. Phung, "Multi-objective electric distribution network reconfiguration solution using runner-root algorithm," *Appl. Soft Comput.*, vol. 52, pp. 93–108, Mar. 2017.

[25] S. Mishra, D. Das, and S. Paul, "A comprehensive review on power distribution network reconfiguration," *Energy Syst.*, vol. 8, no. 2, pp. 227–284, 2017.

[26] M. Zhao, Z. Chen, and F. Blaabjerg, "Probabilistic capacity of a grid connected wind farm based on optimization method," *Renew. Energy*, vol. 31, no. 13, pp. 2171–2187, 2006.

[27] H.-T. Zhang, W. Sun, Y. Li, D. Fu, and Y. Yuan, "A fast optimal power flow algorithm using powerball method," *IEEE Trans. Ind. Informat.*, vol. 16, no. 11, pp. 6993–7003, Nov. 2020.

[28] M. Dzamarija and A. Keane, "Autonomous curtailment control in distributed generation planning," *IEEE Trans. Smart Grid*, vol. 7, no. 3, pp. 1337–1345, May 2015.

[29] A. Asrari, T. Wu, and S. Lotfifard, "The impacts of distributed energy sources on distribution network reconfiguration," *IEEE Trans. Energy Convers.*, vol. 31, no. 2, pp. 606–613, Jan. 2016.

[30] E. Zitzler and L. Thiele, "Multiobjective optimization using evolutionary algorithms—A comparative case study," in *Proc. Int. Conf. Parallel Problem Solving Nat.*, 1998, pp. 292–301.

[31] X. Su, M. A. S. Masoum, and P. J. Wolfs, "PSO and improved BSFS based sequential comprehensive placement and real-time multi-objective control of delta-connected switched capacitors in unbalanced radial MV distribution networks," *IEEE Trans. Power Syst.*, vol. 31, no. 1, pp. 612–622, Mar. 2016.

[32] M. Laumanns and J. Ocenasek, "Bayesian optimization algorithms for multi-objective optimization," in *Proc. Int. Conf. Parallel Problem Solving Nat.*, 2002, pp. 298–307.

[33] S. K. Biswas, A. Rauniyar, and P. K. Muhuri, "Multi-objective Bayesian optimization algorithm for real-time task scheduling on heterogeneous multiprocessors," in *Proc. IEEE Congr. Evol. Comput. (CEC)*, 2016, pp. 2844–2851.

[34] G. F. Cooper and E. Herskovits, "A Bayesian method for the induction of probabilistic networks from data," *Mach. Learn.*, vol. 9, no. 4, pp. 309–347, 1992.

[35] K. Yoon, "Systems selection by multiple attribute decision making," Ph.D. dissertation, Kansas State Univ., Manhattan, KS, USA, 1981.

[36] A. Zhou, B. Qu, H. Li, S. Zhao, P. N. Suganthan, and Q. Zhang, "Multiobjective evolutionary algorithms: A survey of the state of the art," *Swarm Evol. Comput.*, vol. 1, no. 1, pp. 32–49, 2011.
[37] R. D. Zimmerman, C. E. Murillo-Sánchez, and D. Gan, *MATPOWER: A MATLAB Power System Simulation Package*, Power Syst. Eng. Res. Center, Ithaca, NY, USA, 1997.
[38] J. Bader and E. Zitzler, "HYPE: An algorithm for fast hypervolume-based many-objective optimization," *Evol. Comput.*, vol. 19, no. 1, pp. 45–76, 2011.
[39] M. D. A. C. E Silva, C. E. Klein, V. C. Mariani, and L. dos Santos Coelho, "Multiobjective scatter search approach with new combination scheme applied to solve environmental/economic dispatch problem," *Energy*, vol. 53, pp. 14–21, May 2013.
[40] S. Lei, C. Chen, Y. Song, and Y. Hou, "Radiality constraints for resilient reconfiguration of distribution systems: Formulation and application to microgrid formation," *IEEE Trans. Smart Grid*, vol. 11, no. 5, pp. 3944–3956, Sep. 2020.
[41] M. Lange, "On the uncertainty of wind power predictions analysis of the forecast accuracy and statistical distribution of errors," *J. Solar Energy Eng.*, vol. 127, no. 2, pp. 177–184, 2005.
[42] M. Abido, "Optimal power flow using particle swarm optimization," *Int. J. Elect. Power Energy Syst.*, vol. 24, no. 7, pp. 563–571, 2002.
[43] H. Yu, C. Chung, K. Wong, H. Lee, and J. Zhang, "Probabilistic load flow evaluation with hybrid latin hypercube sampling and cholesky decomposition," *IEEE Trans. Power Syst.*, vol. 24, no. 2, pp. 661–667, Mar. 2009.

Tianwei Zhong received the B.E. and M.E. degrees from the Huazhong University of Science and Technology, Hubei, China, in 2018 and 2020, respectively. He is currently a Software Engineer. His research interests include multiobjective optimization, swarm intelligence, and machine learning with applications to power system operation and dispatch.

Hai-Tao Zhang (Senior Member, IEEE) received the B.E. and Ph.D. degrees from the University of Science and Technology of China, Hefei, China, in 2000 and 2005, respectively. From January 2007 to December 2007, he was a Postdoctoral Researcher with the University of Cambridge, Cambridge, U.K. Since 2005, he has been with the Huazhong University of Science and Technology, Wuhan, China, where he was an Associate Professor from 2005 to 2010, and has been a Full Professor since 2010. He is a Cheung Kong Young Scholar. His research interests include swarming intelligence, model predictive control, and unmanned system cooperation control. He is/was an Associate Editor of IEEE TRANSACTIONS ON SYSTEMS, MAN, AND CYBERNETICS: SYSTEMS, IEEE TRANSACTIONS ON CIRCUITS AND SYSTEMS—PART II: EXPRESS BRIEFS, *Asian Journal of Control*, IEEE Conference on Decision and Control, and *American Control Conference*.

Yuanzheng Li (Member, IEEE) received the M.S. degree in electrical engineering from the Huazhong University of Science and Technology, Wuhan, China, in 2011, and the Ph.D. degree in electrical engineering from the South China University of Technology, Guangzhou, China, in 2015. He has published several peer-reviewed papers in international journals. His current research interests include artificial intelligence and its application in smart grid, optimal power system dispatch and decision making, stochastic optimization considering large-scale integration of renewable energy into the power system, and multiobjective optimization.

Lan Liu received the B.E. degree from Wuhan University, China, in 2003, and the Ph.D. degree from the University of Minnesota in 2016. She is currently an Associate Professor with the National Engineering Laboratory for Educational Big Data, Central China Normal University. Her research interests include big data, data visualization, and e-learning.

Renzhi Lu (Member, IEEE) received the B.S. degree from the School of Information Science and Engineering, Wuhan University of Science and Technology, Wuhan, China, in 2014, and the Ph.D. degree from the Department of Electronic Systems Engineering, Hanyang University, Ansan, South Korea. He is currently an Assistant Professor with the School of Artificial Intelligence and Automation, Huazhong University of Science and Technology, Wuhan. His research interests include artificial intelligence (deep reinforcement learning), smart manufacturing (unmanned system cooperation control), and smart grid (energy management). He is a a Member of the IEEE Industrial Electronics Society, the IEEE Computational Intelligence Society, and the IEEE Power & Energy Society.